First Principles Calculation of the Thermodynamic Properties of Silicon Clusters

ARTICLE *in* THEORETICAL CHEMISTRY ACCOUNTS · FEBRUARY 1970

Impact Factor: 2.23 · DOI: 10.1007/s002140050298 · Source: CiteSeer

2 AUTHORS, INCLUDING:

James R. Chelikowsky
University of Texas at Austin
455 PUBLICATIONS **15,261** CITATIONS

First Principles Calculation of the Thermodynamic Properties of Silicon Clusters

David W. Dean and James R. Chelikowsky

Department of Chemical Engineering and Materials Science

Minnesota Supercomputer Institute

University of Minnesota, Minneapolis, MN 55455-0132

(December 17, 1997)

Abstract

The thermodynamic properties of Si clusters are calculated using first principles quantum methods combined with molecular dynamics for simulating the trajectories of clusters. A plane wave basis is used with *ab initio* pseudopotentials and the local density approximation for determining the electronic energies and forces. Langevin molecular dynamics simulates thermal contact with a constant temperature reservoir. Vibrational spectra, moments of inertia, anharmonic corrections, and free energies are predicted for Si_2 through Si_5. The translational contribution is based on the ideal gas limit. The rotation contribution is approximated using a classical rigid rotator. Vibrational modes are determined from the dynamical matrix in the harmonic approximation. Corrections due to anharmonicity and coupling between rotational and vibrational modes are fit from the molecular dynamics simulations.

Key words: Cluster thermodynamics - Pseudopotentials - Molecular dynamics - Silicon clusters.

I. INTRODUCTION

The thermodynamic properties of clusters are of importance to the prediction of nucleation rates and cluster size distributions in vapor condensation. This predictive ability is required to design systems intended to produce such clusters for manufacturing. These systems typically consist of expansion nozzles in which the plasma condenses into clusters [1]. Unfortunately, experimental techniques are not available that can produce a sufficient quantity of size selected clusters to measure their thermodynamic properties. As a consequence, nucleation models depend on theoretical predictions of the cluster free energies. However, reliable and accurate methods for predicting thermodynamic properties are not readily available.

The standard reference for the thermodynamic properties of atomic Si, Si_2, Si_3, and bulk phases is the JANAF tables [2]. These tables use simple analytic methods combined with limited experimental data to estimate thermodynamic properties. For example, Si_3 is assumed to be a linear cluster in the treatment of vibrational and rotational modes. This assumption reassigns one degree of freedom from rotation to vibration in contrast to quantum calculations which give a triangular structure [4]. The redistribution of contributions to the heat capacity and free energies can make dramatic differences.

Alternative approaches to cluster thermodynamics based on classical pair potentials combined with molecular dynamics (MD) or Monte Carlo constitute the bulk of the prior work on predicting cluster thermodynamics [5–12]. *Ab initio* electronic structure and MD methods are frequently used to determine the zero temperature geometry and properties [4,13–16].

Classical nucleation theory assumes that the free energy dependence on size can be characterized by surface ($N^{2/3}$) and volume (N) terms (where N is the number of constituents of the cluster). This approach must break down below sizes in which the cluster can no longer be considered simply a fragment of the bulk material. This is precisely the range of importance to the nucleation of clusters.

Modern electronic structure methods combined with MD or Monte Carlo simulations

offer the potential to predict these properties reliably. However, limitations of available computing power have hindered the exploitation of this approach for the range of cluster sizes and simulation times necessary.

The purpose of our work is to implement existing pseudopotential electronic structure methods combined with Langevin MD for the purpose of predicting the thermodynamic properties of Si clusters. This effort develops the necessary techniques and avoids potential numerical errors associated with the use of these methods for this purpose. Extension of our approach to larger systems will be a simple exercise as computing power becomes available.

Our approach resolves the thermodynamic properties into contributions due to the binding energy, translational and rotational motion, and vibrational modes. Contributions due to electronic excitations are not calculable with the electronic structure methods we employ (i.e. density functional theory) and are neglected. The translational and rotational contributions are well described by classical statistical mechanics and this approach is adopted for these terms. The translational term represents a dominant contribution to the free energies and differences in free energies for small clusters. The vibrational modes determined from the electronic structure methods are combined with quantum statistical mechanics. This approach is necessary to give the proper low temperature behavior which is not accounted for in MD.

All deviations from ideal harmonic behavior evident from the molecular dynamics simulations, are combined in an anharmonic contribution. These deviations include the coupling between rotational and vibrational modes, liquid-like states, transitions between cluster polymorphs, as well as the non-linearity of the effective interaction potential between atoms.

We identified and corrected an artifact associated with the use of numerical methods for evaluation of local contributions to the Hamiltonian. When evaluated on a real space grid, these contributions produce a background potential and gives rise to anomalous heat capacities as the temperature is reduced.

An alternative expression relating heat capacities to energy variations in the MD is examined. For the simulation times and parameters used in this work, this expression does

not provide a reliable estimate of the heat capacity and we do not use it to determine the free energies. However, this approach does give insight into trends and provides a means of estimating the effects of correlation between vibrational and rotational modes.

II. METHODS

The thermodynamic properties of a macroscopic ensemble of clusters of a given size are determined by the total energy dependence on configuration and the relative phase space of these configurations. This energy dependence includes contributions from the kinetic energy of the constituent nuclei, the electrostatic interaction between nuclei, and the electronic energy states of the electrons. The later two terms are associated with the potential energy dependence on structure and the contribution from electronic excitations.

Calculations of thermodynamic properties from this energy dependence may proceed either analytically from a knowledge of the partition function over the phase space of a cluster, or statistically from a sample of the phase space. For clusters of more than a few atoms, the complete phase space of all possible configurations is unmanageably large, and, therefore, unknown. Molecular dynamics and Monte Carlo simulations can be used to provide a statistical sample of this phase space. The potential energy associated with each configuration sampled may be determined from either a quantum calculation of the electronic energy state, or a fitted classical potential.

Our work employs MD combined with a quantum calculation of the electronic ground state based on *ab initio* pseudopotentials [17]. We use the Ceperley-Alder results from Monte Carlo simulations of a homogeneous electron gas [18,19] as parameterized by Perdew and Zunger [20] for the exchange-correlation potential. The Hartree term also depends only on the total electron density:

$$\nabla^2 V_H = -4\pi\rho(\boldsymbol{r}). \tag{1}$$

The basis set used here expands the single-electron wave function in plane waves in a periodic supercell containing the cluster:

$$\psi_{\mathbf{k}}(\mathbf{r}) = \sum_j a(\mathbf{G}_j, \mathbf{k}) e^{i(\mathbf{G}_j + \mathbf{k})\cdot \mathbf{r}}, \tag{2}$$

where $\mathbf{k}$ are wave vectors, and $\mathbf{G}_j$ are the reciprocal lattice vectors of the periodic supercell. This supercell geometry allows the use of well established energy band codes. The charge density used in the Hartree and exchange-correlation terms is iteratively converged to self-consistency from the wavefunctions.

The pseudopotential method accounts for the effects of the chemically inert core electrons by means of an "ion core" potential as seen by the valence electrons. Use of this pseudopotential eliminates consideration of the core states and reduces the computational effort applied to the valence states. The valence wavefunctions outside the core region and eigenvalues for the isolated atom are preserved with this method. Within the core region, relatively smooth pseudowavefunctions replace the more complex all–electron wavefunctions. The radial Kohn-Sham equation in atomic units (a.u.),

$$\left[-\frac{1}{2}\frac{d^2}{dr^2} + \frac{l(l+1)}{2r^2} + V_{tot}[r; \rho(\boldsymbol{r})] \right] r R_{nl}(r) = \epsilon_{nl} R_{nl}(r), \tag{3}$$

is inverted to give the screened pseudopotential:

$$V^{PP}_{scr,l}(r) = \epsilon_l - \frac{l(l+1)}{2r^2} + \frac{1}{2r R^{PP}_l(r)} \frac{d^2}{dr^2} \left[r R_{nl}(r) \right]. \tag{4}$$

The screening is removed by subtracting the Hartree and exchange-correlation potentials as calculated from the pseudowavefunctions,

$$V^{PP}_{ion,l}(r) = V^{PP}_{scr,l}(r) - V^{PP}_H(r) - V^{PP}_{xc}(r). \tag{5}$$

Each angular momentum state (l), produces a different pseudopotential. The ionic pseudopotential operator is then given by:

$$\hat{V}^{PP}_{ion}(r) = V^{PP}_{ion,local}(r) + \sum_l \Delta V_l^{PP}(r) \hat{P}_l, \tag{6}$$

where $V^{PP}_{ion,local}(r)$ is a local potential,

$$\Delta V_l^{PP}(r) = V^{PP}_{ion,l}(r) - V^{PP}_{ion,local}(r) \tag{7}$$

is the semilocal potential for angular momentum l, and $\hat{P}_l$ projects out the lth angular momentum component of the wavefunction. One of the ionic pseudopotentials $V_{ion,l}^{PP}(r)$ is chosen to serve as the local potential.

The pseudopotentials for this work on Si were generated by the method of Troullier and Martins [21,22]. A common core radius of 2.25 a_0 (a_0 = 0.529 Å) was used for s, p and d angular momentum states. The pseudopotential for the p state was used as the local potential.

The nuclei follow classical trajectories in the MD simulation. Additional forces are required to impose thermodynamic equilibrium with a reservoir at a definite temperature. This work uses Langevin dynamics [23] for this purpose. The Langevin dynamics equation of motion is

$$M_I \ddot{\mathbf{R}}_I = \mathbf{F}_I = -\nabla_{\mathbf{R}_I} E\left(\{\mathbf{R}_I\}\right) - \gamma M_I \dot{\mathbf{R}}_I + \mathbf{G}_I, \tag{8}$$

where $E\left(\{\mathbf{R_I}\}\right)$ is the total energy. The fluctuation forces, $\{\mathbf{G_I}\}$, are random Gaussian variables. The dissipative friction factor, γ, defines the magnitude of these fluctuations:

$$\langle G_I^\alpha(t) G_J^\alpha(t') \rangle = 2\gamma M_I k_B T \delta_{IJ} \delta(t - t'), \tag{9}$$

where α is the Cartesian direction index. The Hellmann-Feynman forces, $-\nabla_{\mathbf{R}_I} E\left(\{\mathbf{R}_I\}\right)$, are determined directly from the plane wave expansions [24].

III. APPLICATION TO CLUSTER THERMODYNAMICS

The computational methods described above provide a means of modeling clusters in thermodynamic equilibrium with a fixed temperature environment. The phase space of a given size cluster can be sampled by either a large number of relatively short simulations, or a single long simulation as used in this work. Sufficiently large samples are statistically equivalent to a macroscopic ensemble of clusters at a single point in time (ergodic). The statistical sample must be large enough to sample all regions of the cluster phase space that

contribute significantly to the partition function. The configuration space grows factorially with cluster size, and there may exist low energy regions that are isolated by high energy barriers. A systematic exploration of all configurations is not practical for clusters of more than a couple of atoms. We rely on the MD simulation to access the important minima.

All thermodynamic properties can be calculated from the heat capacity over the temperature range of interest. Statistical ensembles provide predictions of the heat capacity by two methods. The most direct is to differentiate the energy as a function of temperature. The second relates the heat capacity to the variation of energy at each temperature [25]:

$$C_V = \left(\frac{\partial U}{\partial T}\right)_V = \frac{\langle (E - \langle E \rangle)^2 \rangle}{k_B T^2}. \tag{10}$$

The latter method suffers from contributions to the variation in energy due to numerical uncertainties in energy. In addition, this method requires larger samples to provide statistically significant results. The direct approach provides a more reliable prediction of heat capacity from our simulations.

The energy and heat capacity can be separated into the component degrees of freedom.

$$E_{tot} = E_{tran} + E_{rot} + E_{vib\ kin} + E_{pot}. \tag{11}$$

$$C_V = C_{tran} + C_{rot} + C_{vib\ kin} + C_{pot}. \tag{12}$$

The potential and vibrational kinetic terms together form the total vibrational contribution.

Use of Eq. (11) in Eq. (10) relates the variations and correlations for the degrees of freedom to heat capacity:

$$C_V = \sum_i \frac{\langle (E_i - \langle E_i \rangle)^2 \rangle}{k_B T^2} + \sum_{i \neq j} \frac{\langle (E_i - \langle E_i \rangle)(E_j - \langle E_j \rangle) \rangle}{k_B T^2}, \tag{13}$$

where $i, j = tran, rot, vib\ kin, pot$. The terms in the second summation represents the correlations between the degrees of freedom. When the correlations are negligible, the terms in the first summation provide the component heat capacities directly.

In the dilute limit, the contribution to the thermodynamic properties due to the translational degrees of freedom follows ideal gas behavior. The simulation results are consistent

with ideal gas behavior and justify the use of this approach. We did not consider the dense concentration limit. To model the non-ideal behavior in this limit would require simulation of a prohibitively large number of clusters.

For an ideal gas of Si clusters consisting of N atoms each, the translational contributions to the energy, heat capacity and Helmholtz free energy are given by the following expressions [25]:

$$U_{tran} = \frac{3}{2} k_B T. \tag{14}$$

$$C_{tran} = \frac{3}{2} k_B. \tag{15}$$

$$A_{tran} = k_B T \left\{ \ln \left[\left(\frac{2\pi\hbar}{N m_{Si} k_B T} \right)^{\frac{3}{2}} \frac{p}{k_B T} \right] - 1 \right\}. \tag{16}$$

The instantaneous rotational kinetic energy of a cluster is given by an expression involving the principal moments of inertia $I_{p\,i}$ and corresponding angular momenta P_i:

$$E_{rot} = \frac{1}{2} \sum_{i=1}^{3} \frac{P_i^2}{I_{p\,i}}. \tag{17}$$

The principal axes and moments of inertia are the eigenvalues and eigenvectors of the moment of inertia tensor [26]:

$$\boldsymbol{I} = \sum_{n=1}^{N} m_{Si} \left(r_{cm\,n}^2 \mathbf{1} - \boldsymbol{r_{cm\,n} r_{cm\,n}} \right) \tag{18}$$

In the general case of an asymmetric cluster, the three principal moments of inertia are all different. Neither the quantum states, nor the resultant partition function of such an asymmetric top, can be expressed analytically. Numerical methods are available for determining these energies [27–29]. The effects of the quantization of rotational energies are important only at very low temperatures (< 50 K). For this reason, we used the classical limit for rigid clusters and the classical behavior from the MD simulations to determine the rotational contributions to the thermodynamic properties [30]:

$$A_{rot} = -k_B T \ln \left[\frac{\pi^{\frac{1}{2}}}{\sigma} \prod_i \left(\frac{2 I_{p\,i} k_B T}{\hbar^2} \right)^{\frac{1}{2}} \right], \tag{19}$$

$$C_{rot} = \frac{3}{2} k_B, \tag{20}$$

for $N \geq 3$, where σ is the symmetry number equal to the number of rotational elements of the point group for the cluster. For $N = 2$

$$A_{rot\ Si2} = -k_B T \ln\left(\frac{1}{\sigma}\frac{2I_p k_B T}{\hbar^2}\right), \tag{21}$$

$$C_{rot\ Si2} = k_B. \tag{22}$$

At higher temperatures, the clusters do not behave as rigid rotators and the coupling between vibrational and rotational modes may be significant. Fortunately, these effects are significant at temperatures in which the cluster behaves classically. The MD simulations should therefore account for such effects. The rotational energy is calculated directly from the MD results as follows:

$$\boldsymbol{L} = \sum_{n=1}^{N} m_{Si}\ \boldsymbol{r_{cm\,n}} \times \boldsymbol{v_{cm\,n}}, \tag{23}$$

$$I = \sum_{n=1}^{N} m_{Si}\left(\boldsymbol{r_{cm\,n}} \times \frac{\boldsymbol{L}}{L}\right)^2, \tag{24}$$

$$E_{rot} = \frac{1}{2}\frac{L^2}{I}, \tag{25}$$

where $\boldsymbol{L}$ is the angular momentum vector, and I is the moment of inertia along $\boldsymbol{L}$.

The vibrational contribution to the thermodynamic properties derives from highly coupled potential and vibrational kinetic forms of energy. The electronic energy gives rise to a potential that depends on the relative positions of the constituent atoms. The vibrational kinetic energy can be obtained directly from the MD and should obey the law of equipartition in the classical limit.

At low temperatures, the cluster is a solid-like linear harmonic oscillator. At these temperatures, the quantization of vibrational states has a significant effect on the thermodynamic properties. Classical MD cannot reproduce these effects directly. Instead, we determine the force constants for the dynamical matrix from static simulations and calculate the properties analytically.

The vibrational frequencies ω are the eigenvalues of the dynamical matrix $\mathbf{M}$,

$$\mathbf{M}\boldsymbol{\Delta}\mathbf{r} = -m_{Si}\ \omega^2 \boldsymbol{\Delta}\mathbf{r}, \tag{26}$$

where $\Delta r_{m\,i}$ is the displacement from the equilibrium position of atom m along direction i. The elements of the dynamical matrix are given by:

$$M_{m\,n\,i\,j} = \frac{\partial F_{m\,i}}{\partial \Delta r_{n\,j}}, \tag{27}$$

where $F_{m\,i}$ is the force on atom m along direction i.

These frequencies determine the vibrational contributions to the free energy [25],

$$A_{vib} = \sum_{k=1}^{3N-6} \left[\frac{\hbar\omega_k}{2} + k_B T \ln\left(1 - e^{-\frac{\hbar\omega_k}{k_B T}}\right)\right]; \tag{28}$$

and the heat capacity,

$$C_{vib} = k_B \sum_{k=1}^{3N-6} \frac{\left(\frac{\hbar\omega_k}{k_B T}\right)^2 e^{-\frac{\hbar\omega_k}{k_B T}}}{\left(1 - e^{-\frac{\hbar\omega_k}{k_B T}}\right)^2}\,. \tag{29}$$

At elevated temperatures, the cluster displays anharmonic behavior and eventually approaches a liquid-like state. The coupling between rotational and vibrational modes becomes more pronounced at high temperatures. The MD simulations account for these effects within the important high temperature classical limit. The differences between the potential energy and heat capacity from the MD results, and the theoretical results for a classical linear harmonic oscillator are due to these effects. We fit the energy difference to a low order polynomial,

$$U_{anh} = U_{pot} - \frac{3N-6}{2} k_B T = \sum_{n\geq 0} c_n T^{n+2}, \tag{30}$$

with the requirement that the anharmonic contribution to the heat capacity approach zero at 0 K,

$$C_{anh} = \sum_{n\geq 0} (n+2) c_n T^{n+1}. \tag{31}$$

This latter requirement applies to the classical oscillator but also satisfies the quantum result that all contributions to the heat capacity must be zero at 0 K. The correction to the free energy needed to account for these effects is then given by:

$$A_{anh} = -\sum_{n\geq 0} \frac{c_n}{n+1} T^{n+2}. \tag{32}$$

A greater number of temperature points could allow the use of higher order fits. For larger clusters, the transition to liquid-like behavior can result in more complex heat capacity trends. In the bulk limit, the transitions are abrupt, and the heat capacity is discontinuous, with a latent heat associated with the transition temperature.

An expression for the thermodynamic properties of a dimer is available based on an approximation to the quantum mechanical partition function [31]. The interaction potential is expanded to third order in separation distance. The coupling between rotational and vibrational modes is based on perturbation theory. The expansion of the interaction potential can be expressed in a form consistent with the Morse potential [32]:

$$E_{pot}(\Delta r) = D_e \left(1 - e^{-\beta \Delta r}\right)^2 = D_e \left[\beta^2 (\Delta r)^2 - \beta^3 (\Delta r)^3 + \cdots\right], \tag{33}$$

where the interatomic force constant $k_e = \left(\frac{d^2 E_{pot}}{dr^2}\right)_{r_e}$ is related to the Morse potential parameters:

$$D_e \beta^2 = \frac{1}{2} k_e. \tag{34}$$

The fundamental vibration frequency and moment of inertia at the equilibrium separation r_e are:

$$\omega_e = \frac{\nu_e}{c} = \frac{1}{2\pi c}\sqrt{\frac{k_e}{\mu}}, \tag{35}$$

$$I_e = \mu r_e^2, \tag{36}$$

where the reduced mass $\mu = \frac{m_{Si}}{2}$. The rotation constant B_e, first anharmonicity constant x_e, and the vibration–rotation interaction constant α_e are defined as:

$$B_e = \frac{\hbar}{4\pi I_e c}, \tag{37}$$

$$x_e = \frac{h\nu_e}{4D_e}, \tag{38}$$

$$\alpha_e = 6\frac{B_e^2}{\omega_e}\left(\sqrt{\frac{\omega_e x_e}{B_e}} - 1\right). \tag{39}$$

With these approximations the free energy and heat capacity are given by:

$$A_{anh\ Si2} = k_B T \left[\frac{8\gamma}{u} + \frac{\delta}{e^u - 1} + \frac{2x_e u}{(e^u - 1)^2} \right], \tag{40}$$

$$C_{anh\ Si2} = k_B \left[\frac{16\gamma}{u} + \frac{\delta u^2 e^u}{(e^u - 1)^2} + \frac{u^2 e^u (2\delta e^u - 4x_e u - 8x_e)}{(e^u - 1)^3} + \frac{12 x_e e^{2u}}{(e^u - 1)^4} \right], \tag{41}$$

where

$$\gamma = \frac{B_e}{\omega_e}, \tag{42}$$

$$u = \frac{h\nu_e}{k_b T} (1 - 2x_e), \tag{43}$$

$$\delta = \frac{\alpha_e}{B_e}. \tag{44}$$

A quantum statistical mechanics approach to anharmonicity and bending mode coupling with rotation for linear triatomic systems is also available [33]. For such linear triatomic systems, this approach provides an alternative method to estimate such effects.

The Gibbs free energy is of interest in situations involving equilibrium between clusters of different sizes (e.g. situations such as found in a Si plasma expansion nozzle). The pressure-volume work term associated with the Gibbs free energy is not directly accessible from our MD results. Instead, we use the dilute ideal gas limit for this contribution with

$$pV = k_B T. \tag{45}$$

At relatively high temperatures, depending on the excitation energies, electronic excitations can contribute to the thermodynamic properties. The energy levels available for excited states depend strongly on the configuration of the cluster. This dependence couples the vibrational and electronic modes. Excited states cannot be easily determined using density functional theory. Treatment of excited states falls outside the scope of this work.

IV. COMPUTATIONAL TECHNIQUES

Any numerical solution to a set of integral-differential equations introduces computational approximations. These approximations can manifest themselves in anomalous predictions

and guide the choice of precision in the various modeling parameters. For example, the local contributions to the Hamiltonian are evaluated on a discrete real space grid. These contributions include the local part of the pseudopotential, the exchange-correlation potential, and the Hartree term. Within this approximation, the energies become dependent on the position and orientation of the cluster with respect to the grid. This variation corresponds to a real space periodic potential that is fixed to the supercell rather than to the cluster. The effect can be clearly illustrated with a single Si atom. Physically a single Si should see no external potential, even accounting for image effects from the repeating supercell. However, the simulation cases clearly show a periodic "egg-crate" potential, when the Si is translated (see Figure 1).

This artificial background potential gives rise to an additional three translational and three rotational degrees of freedom in energy. Unless the temperature is large compare to these potential wells, the additional degrees of freedom contribute to the heat capacity. The magnitude of this effect in terms of temperature can be seen by reference to the right hand scale shown in Figure 1. In the low temperature classical harmonic limit these six additional degrees of freedom should add $3k_B$ to the heat capacity.

Initial results with MD simulations showed this anomalous low temperature heat capacity associated with potential energy (see Figure 2). These preliminary cases differ from the final set in that they are run for only 200 rather than 4000 time steps. With this few steps, the statistics are less stable. However, the anomalous low temperature heat capacity is clearly evident.

The grid spacing is determined from the number of sample points required to use a fast Fourier transform evaluation of the local terms with a cutoff corresponding to that used in the plane wave expansion. Therefore, the magnitude of the effect at finite temperatures can be reduced by increasing the cutoff in the plane wave expansion. However, this approach only lowers the temperature range over which the effect is important, and does so at a high computational cost. A more direct approach to removing the degrees of freedom is to use a separate real space coordinate system, attached to the cluster, for the plane wave calculation

of forces and energies. This coordinate system would translate and rotate with the cluster within the fixed coordinates used in the MD calculation of trajectories. A form of this approach is used to remove this effect.

Ideally, one would like to have the plane wave coordinates translate and rotate along with the cluster of atoms. With respect to translation, this approach is simple to implement by fixing the coordinates with the center of mass. For rotation, this approach cannot be used in a physically simple way. The rotational motion of asymmetric and non-rigid bodies cannot be described analytically, and the numerical integration of the equations of motion used in MD do not rigorously conserve angular momentum. For this reason, it is not possible to determine precisely the net rotation of a cluster between consecutive time steps. Attempts to approximate the net rotation lead to long term drift of the coordinates with respect to the cluster, and do not remove effectively the rotational degrees of freedom.

A less physical, but simple and effective approach, is used to remove the rotational degrees of freedom. Three atoms are arbitrarily chosen from the cluster to fix the angular orientation of the coordinates. The first two atoms define a fixed direction. The plane containing all three atoms about this direction fixes the angular position of the coordinates. In addition, the effect of the background potential is reduced by removing the net force and torque on the cluster. This correction is performed without distortion, for the cluster dynamics by determining the resultant translational and rotational acceleration arising from the Hellmann-Feynman forces, and by applying forces that uniformly remove the accelerations. The effectiveness of this approach in removing this artifact can be seen in Figure 2.

Another potential artifact can influence thermodynamic quantities in MD simulations. Discretization of the equations of motion can cause the system to not conserve energy. For example, as a dimer vibrates, the atoms may approach closer than energy conservation would allow if the time steps are too coarse. This effect could increase the vibrational kinetic energy above the thermostat temperature. We chose a time step size of 200 $a.u.$ by running simulations without a thermostat ($\gamma = 0$ in Eq. (8)) to verify that the energy remained conserved. Furthermore, the results of our simulations do not show indication of

any anomalous heating that would result from too coarse a time step.

V. SIMULATIONS

MD simulations are intended to model a cluster in equilibrium with a constant temperature environment. Once a cluster has formed, it requires some time to adjust structurally before it can be said to be in equilibrium. This structure approaches a lowest energy configuration as the temperature is lowered. The lowest energy structure at 0 K is required for determining the dynamical matrix and moment of inertia tensor. These considerations guided the sequence of MD simulation cases run. The various MD cases consume the bulk of the computational resources owing to the large number of time steps required. For these cases, we chose a plane wave cutoff of 9 Ry, and a self-consistency convergence of 0.01 Ry.

The first set of cases is designed to produce the lowest energy structures at 0 K. The structures for Si_2 through Si_5 are shown in Figure 3. Results from Hartree-Fock [13] and pseudopotentials combined with a finite difference calculation [4] are shown for comparison. The atoms of the cluster are initially arranged randomly in a box of size 9.0 a_0 at a temperature of 1500 K. The temperature is then reduced to 0 K in 500 steps of 200 a.u. The last step of this anneal provides the starting point for subsequent simulations. This procedure for determining the minimum energy structure can yield structures that correspond to local minima, but are not a global minimum. Even for a cluster as small as Si_5, a single pass through this procedure did not yield the lowest energy structure. For Si_5, we relaxed the structure determined from earlier work [14] to confirm that it was lower in energy than the one produced by annealing from a high temperature. In general, one should perform several anneals from different initial conditions to find the lowest energy structure.

The most demanding cases are required for determining the thermodynamic statistics. The detail and precision of the statistics are improved with longer simulations at a denser set of temperatures. This study examined a minimal set of four temperatures (500, 1000, 2000, and 3000 K). These cases were run for 4000 time steps of 200 a.u. or a total simulation time

of 19.4 ps. The first 1000 steps were omitted from the statistics to allow for equilibration.

The structure from the anneal is further relaxed for 200 time steps with higher precision simulation parameters (i.e. 32 Ry cutoff and 0.001 Ry convergence) to yield the configuration for calculating the moment of inertia tensor, and the equilibrium positions for the perturbations used to set up the dynamical matrix. The tighter numerical parameters are necessary to obtain sufficient precision in the differences in forces needed in the dynamical equation (Eq. (26)). The perturbation cases involve moving each atom along each direction a small amount in order to obtain the resulting forces. Each atom is displaced along each direction sequentially without returning to its initial position. The final such atom movements correspond to returning the cluster to its initial configuration. This scheme ensures that the results of moving $N-1$ atoms in a single direction is equivalent to moving the remaining atom in the opposite direction. As each displacement is made, the center of mass is fixed by displacing the other atoms together. Any remaining net force and torque must be removed mathematically to avoid spurious vibrational modes of the cluster. Residual torques and forces would cause the cluster to vibrate rigidly as a whole about the initial position and orientation. This procedure can be used to determine the vibrational modes of a cluster of a general shape. However, many clusters possess symmetries that allow for fewer cases to determine the entire dynamical matrix. These symmetries are associated with degeneracies in the vibrational spectrum. The general approach outlined above will split these degeneracies owing to the sequential displacements breaking the symmetry, and the numerical variations between symmetric displacements.

Figure 4 shows the results for a simulation of Si_4 at 3000 K. The variations in energy illustrate the difficulty in obtaining meaningful statistics within within computationally useful time limits. Local energy minima lead to the long term variations in potential energy as the cluster oscillates about the corresponding structures.

VI. ENERGY

An example of the total and component energies averaged from the MD simulations for Si_4 is shown in Figure 4. The lines corresponding to an ideal harmonic gas of clusters provide points of reference.

Although the translational energies from the MD simulations are not used directly for thermodynamic properties, they do confirm the thermostat temperatures for the simulations.

The rotational energies are reasonably close to the ideal classical behavior. This result justifies the use of Equations (19) and (20) with the moments and symmetry numbers given in Table I.

Figure 5 compares JANAF [2] and our results for the rotational contribution to the Gibbs free energy. The Si_2 comparison reflects the close agreement with the moment of inertia of $4.6 \times 10^5\ m_e a_0^2$ reported in JANAF. This value is based on the spectroscopic data from Verma and Warsop [34]. The large differences in Si_3 reflect the assumption of a linear cluster in the JANAF tables. A linear cluster has only two rotational modes, rather than the three modes associated with our non-linear structure.

The vibrational contributions to energy, especially potential energy, show the largest differences from ideal behavior. These differences are due to the non-linear behaviors discussed in Section II, and are accounted for in the anharmonic contributions.

The case of Si_2 allows for an independent method of estimating the vibrational contribution directly from the classical potential energy partition function. The combined rotational, vibrational, and anharmonic correction to the partition function is given by:

$$Z_{comb\ Si2} = Z_{rot\ Si2} Z_{vib\ Si2} Z_{anh\ Si2} = \frac{(\mu k_B T)^{\frac{3}{2}}}{\sigma \hbar^3} \sqrt{\frac{2}{\pi}} \int_0^{R_{max}} \left(\frac{r}{r_e}\right)^2 e^{-\frac{E_{pot}(r)}{k_B T}} dr. \tag{46}$$

By substituting the expressions for the rotational and vibrational partition functions,

$$Z_{rot\ Si2} = \frac{2 I_e k_B T}{\hbar^2}, \tag{47}$$

$$Z_{vib\ Si2} = \frac{k_B T}{h \nu_e}, \tag{48}$$

the anharmonic corrections to the partition function and free energy are obtained:

$$Z_{anh\ Si2} = \sqrt{\frac{k_e}{2\pi k_B T}} \int_0^{R_{max}} \left(\frac{r}{r_e}\right)^2 e^{-\frac{E_{pot}(r)}{k_B T}} dr, \tag{49}$$

$$A_{anh\ Si2} = -k_B T \ln Z_{anh}. \tag{50}$$

Since the potential energy depends only on the separation of the two silicon atoms, the configuration space can be computed easily. The integral must be truncated at some reasonable R_{max} due to the form of the potential. The lowest free energy state for a single dimer in an infinite space is dissociated. The vast number of states available to a disassociated pair contributes an entropy advantage that dominates the free energy. In a physical system, the dimer is confined or in the presence of other clusters, thus limiting the entropy contribution to the free energy. The ensemble average potential energy derives from this partition function:

$$U_{pot} = \frac{\int_0^{R_{max}} E_{pot}(r) \left(\frac{r}{r_e}\right)^2 e^{-\frac{E_{pot}(r)}{k_B T}} dr}{\int_0^{R_{max}} \left(\frac{r}{r_e}\right)^2 e^{-\frac{E_{pot}(r)}{k_B T}} dr}. \tag{51}$$

Numerical integration of Eq. (51) produces the results in Figure 6. The MD results are shown for comparison. The remaining differences with MD are due to a combination of statistical sampling, and the self-consistency convergence variations.

Anharmonic corrections to the free energy are also shown in Figure 6. The correction from the MD simulations, the classical partition functions, and the quantum partition function are based on Equations (32), (50), and (40) respectively. The JANAF [2] results are also based on Eq. (40). The parameters required for Eq. (40) are given below:

$$\omega_e = 442\ \text{cm}^{-1}\ \left(510.98\ \text{cm}^{-1}\right), \tag{52}$$

$$B_e = 0.252\ \text{cm}^{-1}\ \left(0.2390\ \text{cm}^{-1}\right), \tag{53}$$

$$x_e = 0.00787\ \ (0.00395), \tag{54}$$

$$\alpha_e = 0.00234\ \text{cm}^{-1}\ \left(0.0013\ \text{cm}^{-1}\right), \tag{55}$$

where the values enclosed in parentheses are reported in JANAF [2] and are based on the spectroscopic data of Verma and Warsop [34]. Any of these approaches provide a reasonable

estimate for this small correction. For consistency, the MD results are used for the remainder of this work.

The average energies show a roughly symmetric difference from ideal behavior for the rotational and vibrational kinetic energies. This symmetry indicates a correct temperature for the system. Anomalous heating would have tended to raise the vibrational kinetic energy alone.

The vibrational frequencies determined from Eq. (26) are given in Table II. Results from various other calculations and experiment are included. Comparisons between the JANAF [2] and our results for the vibrational contribution to the dimensionless heat capacity, C_V/k_B, are shown in Figure 7. The relatively small differences for Si_2 reflects the vibrational frequency of 510.98 cm^{-1} reported in JANAF. This value is based on spectroscopic data from Verma and Warsop [34]. The dramatic differences in Si_3 are due to the assumption of a linear cluster in the JANAF tables. A linear cluster has two linear vibrational modes and a doubly degenerate bending mode. At high temperatures this difference compensates the difference in the rotational contribution. However, at low temperatures these effects do not cancel due to the drop in vibrational heat capacity.

The difference between the average potential energies and ideal behavior for Si_2 through Si_5 were fit to the form of Eq. (30). Third order fits appear to offer the best compromise for most of these clusters. For Si_5, which lacks a point at 3000 K, the second order fit is a more reasonable choice. These fit coefficients are presented in Table III.

VII. HEAT CAPACITY

For the purpose of investigation, heat capacities are calculated from the variations in component energy in the MD simulations (see Eq. (10)). Graphs of the dimensionless heat capacities of Si_2 are presented in Figure 8.

The difference between the contribution from the potential energy and the ideal behavior is most significant and is not reflected in the change in average potential energy with

temperature. The variations in potential energy are compounded by the self-consistency convergence. The kinetic energy contributions to the heat capacity are consistent with the trends evident in the energy. Vibrational kinetic is slightly higher and rotational is slightly lower than ideal behavior. The translational heat capacity is essentially ideal. The covariance terms are generally small but not all negligible in comparison to the variance terms.

VIII. FREE ENERGY

The methods in Section II are used to construct component Helmholtz and total Gibbs free energies based on the simulation results (see Figure 9). These predictions are close to the values from the JANAF tables. The agreement is not surprising as the dominant term is due to translational energy and the other components are not too far from ideal. The bulk of the remaining difference for Si_2 is due to the neglect of excited electronic states in the current work.

The predictions for Si_5 are limited to 2000 K due to the results of our simulations at the higher temperature. The 3000 K simulation for Si_5 resulted in a disassociated Si atom with a Si_4 cluster. Therefore, this case is not representative of a Si_5 cluster. Only the predictions through 2000 K are used in subsequent calculations. This was the only case that exhibited a disassociation.

From the MD, the more interesting effects are captured in the anharmonic terms, which are a small contribution to the total Gibbs free energy for the clusters considered here. However, the vibrational and associated anharmonic contributions grow in proportion to cluster size and eventually become the dominant contributions to the free energy.

In order to calculate equilibria between clusters of different sizes, the Gibbs free energy should be converted to a per mole of Si basis, rather than per mole of cluster. In addition, the relative binding energies of the clusters must be included. The calculated binding energy for these clusters are given in Table IV. The ground state vibrational energy is included in the vibrational free energy and not included in these bonding energies.

IX. CONCLUSIONS

We have presented the results of calculations of the thermodynamic properties of Si clusters through Si_5, based on MD combined with first principles quantum mechanical methods. These results represent a considerable advance over empirical potentials and provide reliable values where experimental data is unavailable. All parameters needed to calculate thermodynamic properties for Si_2 through Si_5 are presented. Such calculations would have applications in cluster nucleation models.

As available computers become more powerful and computational algorithms become more efficient, the methods developed here can readily be applied to larger clusters. These techniques are also applicable to clusters formed of different species.

ACKNOWLEDGMENTS

We would like to acknowledge support for this work by the Minnesota Supercomputer Institute, the National Science Foundation, and the Department of Energy. One of us (DWD) would like to acknowledge support from Northern States Power Company and the helpful discussions with N. Troullier.

REFERENCES

[1] S. L. Girshick and C.-P. Chiu, Plasma Chem. and Plasma Process. **9**, 355 (1989).

[2] M. W. Chase, C. A. Davies, J. R. Downey, Jr., D. J. Frurip, R. A. McDonald, and A. N. Syverud, *JANAF Thermodynamic Tables*, Third edition, (American Chemical Society and the American Institute of Physics for the National Bureau of Standards, Washington, D. C., 1985).

[3] X. Jing, N. Troullier, J. R. Chelikowsky, K. Wu, and Y. Saad, Solid State Comm. **96**, 231 (1995).

[4] X. Jing, N. Troullier, D. Dean, N. Binggeli, J. R. Chelikowsky, K. Wu, and Y. Saad, Phys. Rev. B **50**, 12234 (1994).

[5] W. D. Kristensen, E. J. Jensen, and R. M. J. Cotterill, J. Chem. Phys **60**, 4161 (1973).

[6] N. Quirke and P. Sheng Chem. Phys. Lett. **110**, 63 (1984).

[7] Z. Li and H. A. Scheraga, J. Chem. Phys **92**, 5499 (1990).

[8] J. P. K. Doyle and D. J. Whales, J. Chem. Phys. **102**, 9659 (1990).

[9] D. J. Whales, Science, **271**, 925 (1996).

[10] K. D. Ball, R. S. Berry, R. E. Kunz, F. Li, A. Prokykova, and D. J. Whales, Science, **271**, 963 (1996).

[11] J. P. Rose and R. S. Berry, J. Chem. Phys **96**, 517 (1992).

[12] J. P. Rose and R. S. Berry, J. Chem. Phys **98**, 3247 (1993).

[13] K. Raghavachari and V. Logovinsky, Phys. Rev. Lett. **55**, 2853 (1985).

[14] J. R. Chelikowsky, N. Binggeli, and K. M Glassford, Zeitschrift für Physik D **26**, 51 (1993).

[15] C. Rohlfing and K. Raghavachari, J. Chem. Phys. **96**, 2114 (1992).

[16] R. Fournier, S. B. Sinnott, and A. E. DePristo, J. Chem. Phys. **97**, 4149 (1992).

[17] M.L.Cohen and J.R.Chelikowsky, "*Ab Initio* Pseudopotentials for Semiconductors," *Handbook on Semiconductors*, ed. P. Landsberg, **1**, 59 (Elsevier,1992).

[18] D.M. Ceperley, Phys. Rev. B **18**, 3126 (1978).

[19] D.M. Ceperley and B.J. Alder, Phys. Rev. Lett. **45**, 566 (1980).

[20] J. P. Perdew and A. Zunger, Phys. Rev. B **23**, 5048 (1981).

[21] N. Troullier and J. Martins, Phys. Rev. B **43**, 1993 (1991).

[22] N. Troullier and J. Martins, Phys. Rev. B **43**, 8861 (1991).

[23] J. C. Tully, G. Gilmer, and M. Shugard, J. Chem. Phys. **71**, 1630 (1979).

[24] J. Ihm, A. Zunger and M.L. Cohen, J. Chem. Phys. **12**, 4409 (1979).

[25] C. Kittel and H. Kroemer, *Thermal Physics*, Second Ed., (W. H. Freeman and Co., San Francisco, 1980).

[26] K. R. Symon, *Mechanics*, Third Ed., (Addison-Wesley Publishing Co., Menlo Park, 1971).

[27] G. W. King, R. M. Hainer, P. C. Cross, J. Chem. Phys. **11**, 27 (1943).

[28] F. Kneubül, T. Gäumann, and Hs. H. Günthard, Journal of Molecular Spectroscopy **3**, 349 (1959).

[29] R. H. Schwendeman, Journal of Molecular Spectroscopy **7**, 280(1961).

[30] D. A. McQuarrie, *Statistical Mechanics*, First Ed., (Harper and Row, New York, 1976).

[31] J. E. Mayer and M. G. Mayer, *Statistical Mechanics*, Second Ed., (John Wiley and Sons, Inc. , New York, 1977).

[32] M. Karplus and R. N. Porter, *Atoms and Molecules: An Introduction for Students*

of Physical Chemistry, (Benjamin/Cummings Publishing Co., Menlo Park, California, 1970).

[33] B. C. Garrett and D. G. Truhlar, J. Phys. Chem. **83**, 1915 (1979).

[34] R. D. Verma and P. A. Warsop, Can. J. Phys. **41**, 152 (1963).

[35] E. C. Honea, A. Ogura, C. A. Murray, K. Raghavachari, O. Sprenger, M. F. Jarrold, and W. L. Brown Nature **366**, 42 (1993).

TABLES

TABLE I. Principal moments of inertia, in units of 10^5 $m_e a_0^2$, and symmetry numbers for Si clusters.

	Si_2	Si_3	Si_4	Si_5
I_1	4.38	10.47	19.23	16.68
I_2	4.38	7.17	14.07	16.30
I_3		3.30	5.16	16.30
σ	2	2	4	6

TABLE II. Eigenmode frequencies in units of cm^{-1} for Si clusters. The column titled P-W is from the current results using Eq. (26). FDP refers to finite difference pseudopotential calculations [3]. H-F are based on Hartree–Fock results [15]. LCAO is from a linear combination of atomic orbital calculations [16]. Doubly degenerate frequencies are indicated by the superscript $*$.

Cluster	Experimental [2,35]	PW	FDP [3]	H-F [15]	LCAO [16]
Si_2	511	442	520		
Si_3		160			
		546			
		577			
Si_4		89	160	117	55
		253	280	305	248
	345	341	340	357	348
		443	460	465	436
	470	471	480	489	464
		504	500	529	495
Si_5		174*	180	170	178
		234	230	201	232
		378*	390	302	377
		418	430	353	409
		438*	450	480	440
		486	490	468	476

TABLE III. Polynomial fit coefficients for anharmonicity of Si clusters, in units of Hartree K^{-n} (see Eq. (30)).

n	Si_2	Si_3	Si_4	Si_5
0	2.4465×10^{-10}	1.6860×10^{-09}	8.9204×10^{-10}	2.0836×10^{-09}
1	-3.0350×10^{-14}	-5.1102×10^{-13}	-7.8848×10^{-15}	

TABLE IV. Binding energy (in kJ/mole Si) for Si clusters.The row titled P-W is from the current results using Eq. (26). H-F are based on Hartree–Fock results [13]. LCAO is from a linear combination of atomic orbitals calculation with gradient corrected density functional theory [16].

	Si_2	Si_3	Si_4	Si_5
P-W	224	327	383	410
H-F [13]	73	97	146	143
LCAO [16]	174	251	298	318
Experiment [2]	149	227		

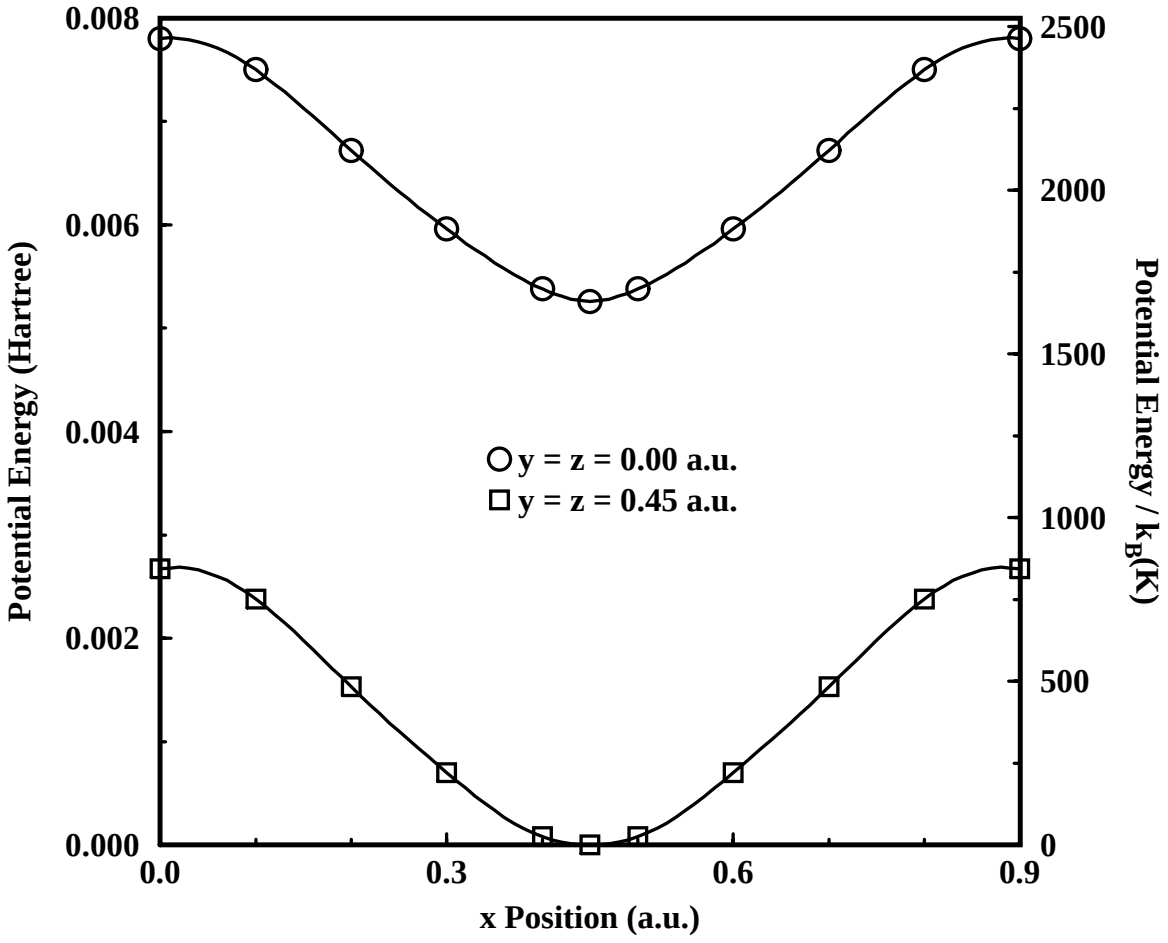

FIG. 1. Potential energy of a Si atom displaced along the x-direction with y and z fixed. The right hand scale converts the potential energy to temperature units in K. The grid spacing of 0.9 a_0 results from a plane wave cutoff of 9 Ry and a 18 a_0 cubic supercell

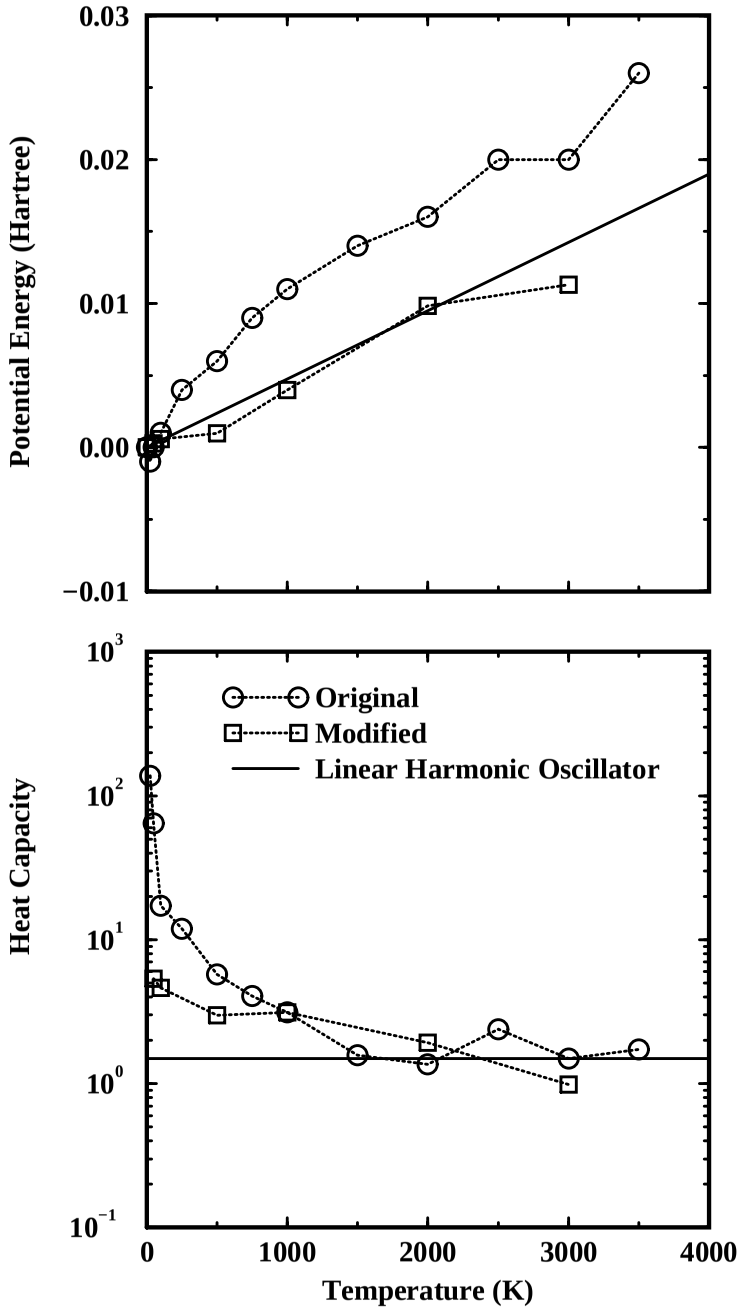

FIG. 2. Potential energy and the associated contribution to the dimensionless heat capacity for Si_3 from molecular dynamics simulations. The heat capacity is based on Eq. (13). The circles and squares correspond to results from original simulations and after the algorithm was modified respectively. The solid lines corresponds to an ideal linear harmonic oscillator.

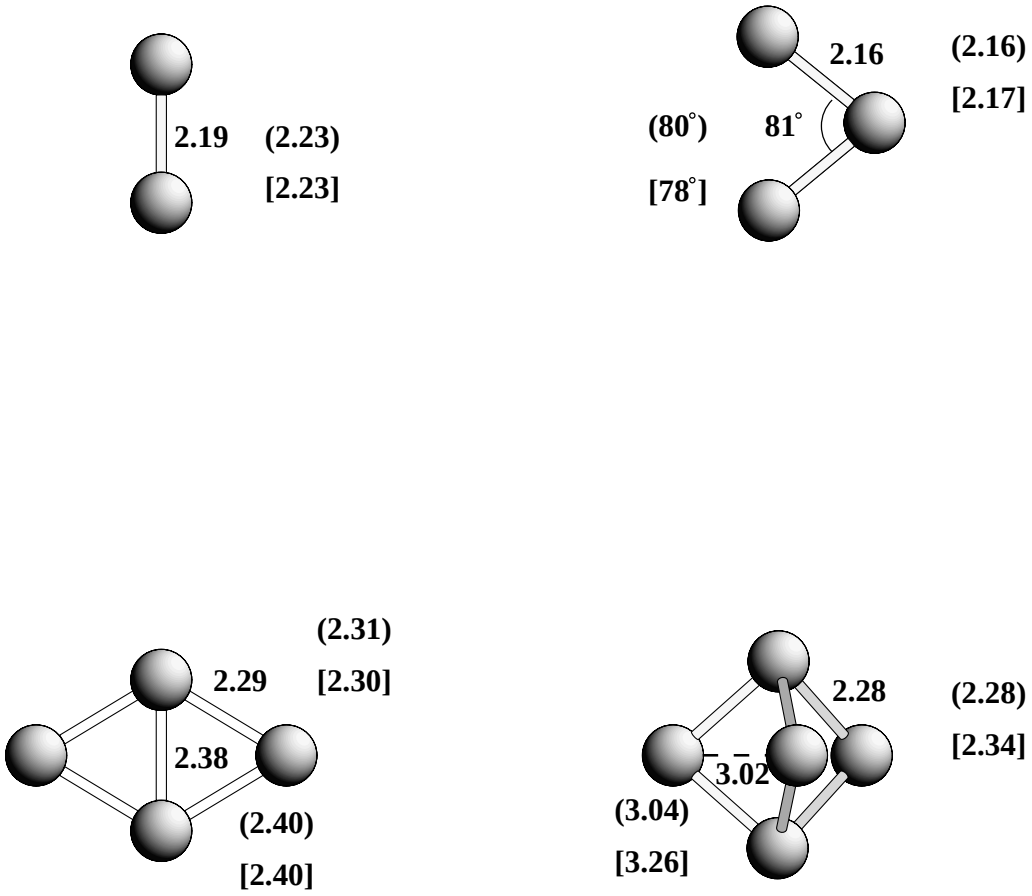

FIG. 3. The the minimum energy structures of Si_2 through Si_5. The interatomic distances are in Å. The values without brackets are from the current work. The values in parenthesis are from pseudopotential finite difference calculations [4] and those in square brackets are from Hartree–Fock calculations [13]

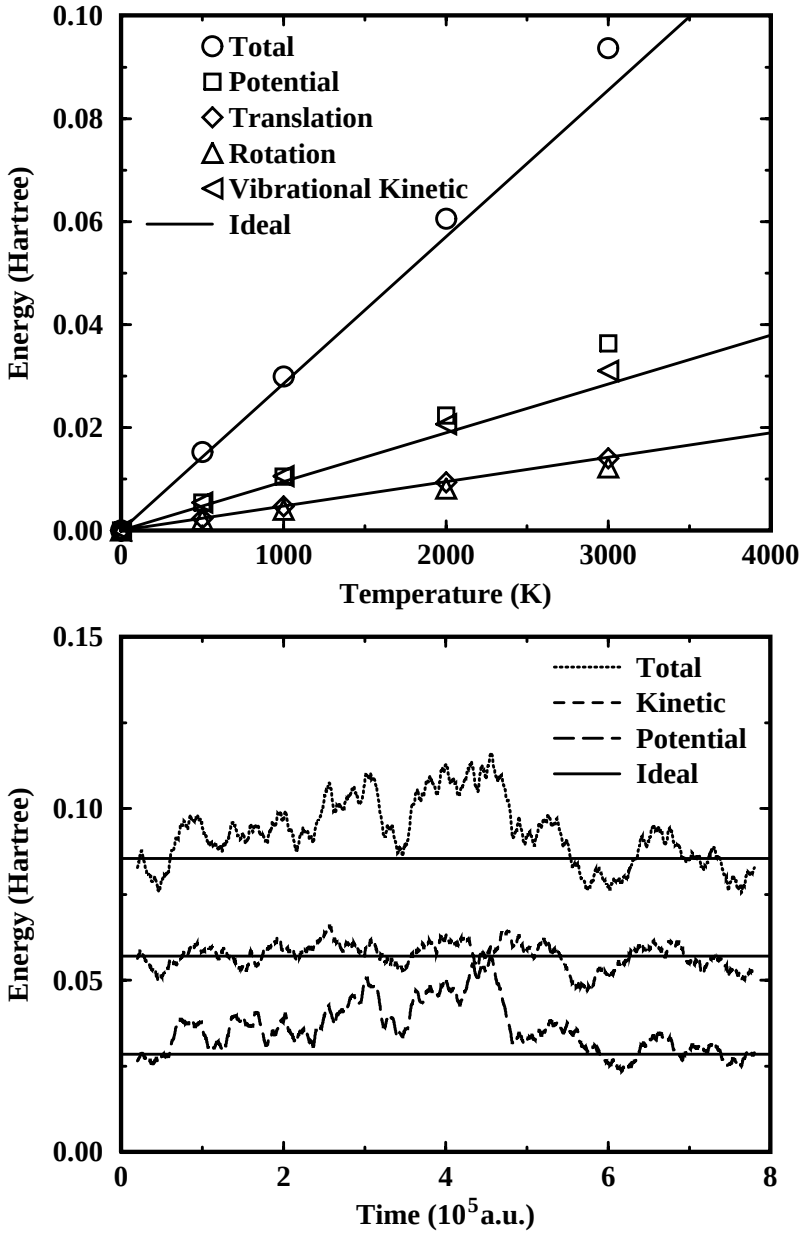

FIG. 4. Average energies of Si_4 from molecular dynamics simulations (upper graph). Running averages of energy from a molecular dynamics simulation of Si_4 at 3000 K (lower graph). The running averages are taken over a centered window of 4×10^4 a.u. The solid lines correspond to an ideal classical gas of clusters that vibrate as linear harmonic oscillators and rotate as rigid rotators.

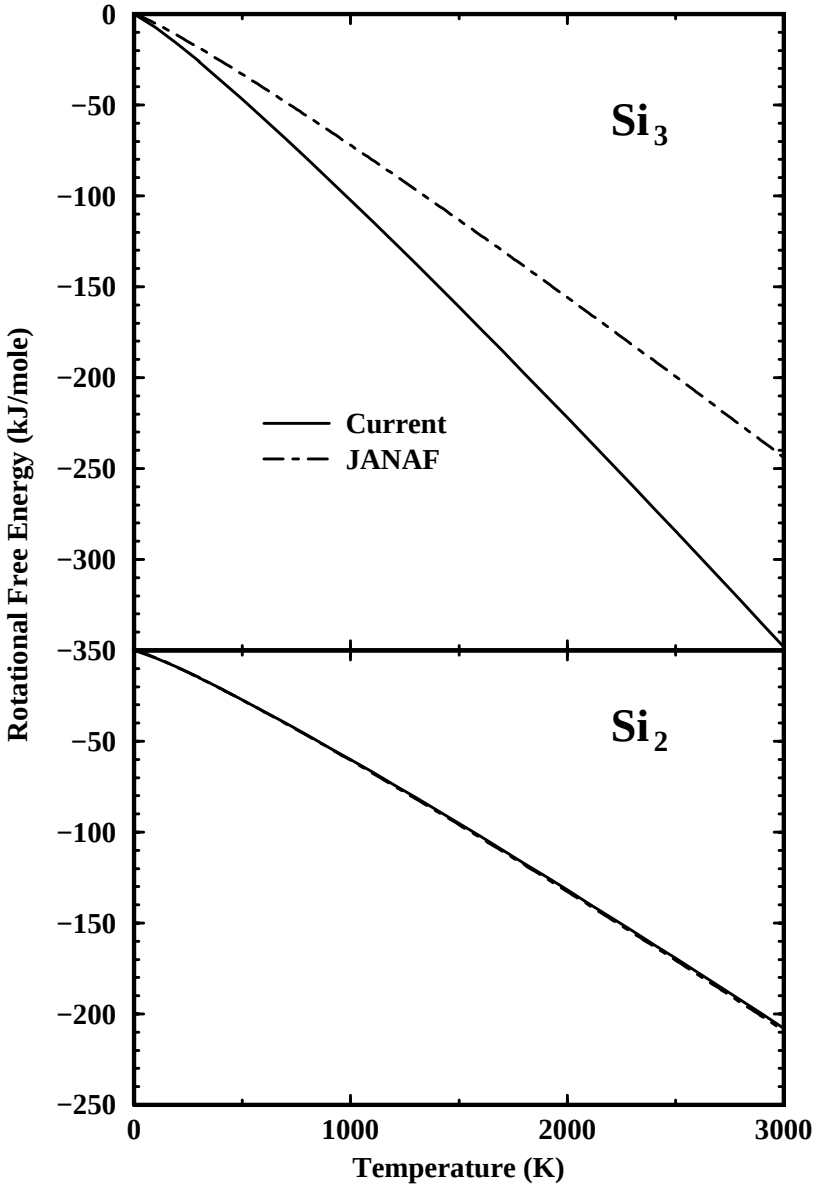

FIG. 5. Rotational contribution to the Gibbs free energy of Si_2 and Si_3 from JANAF [2] and our work. These curves are based on Eq. (19) using the principle moments of inertia from the our calculated structures and JANAF.

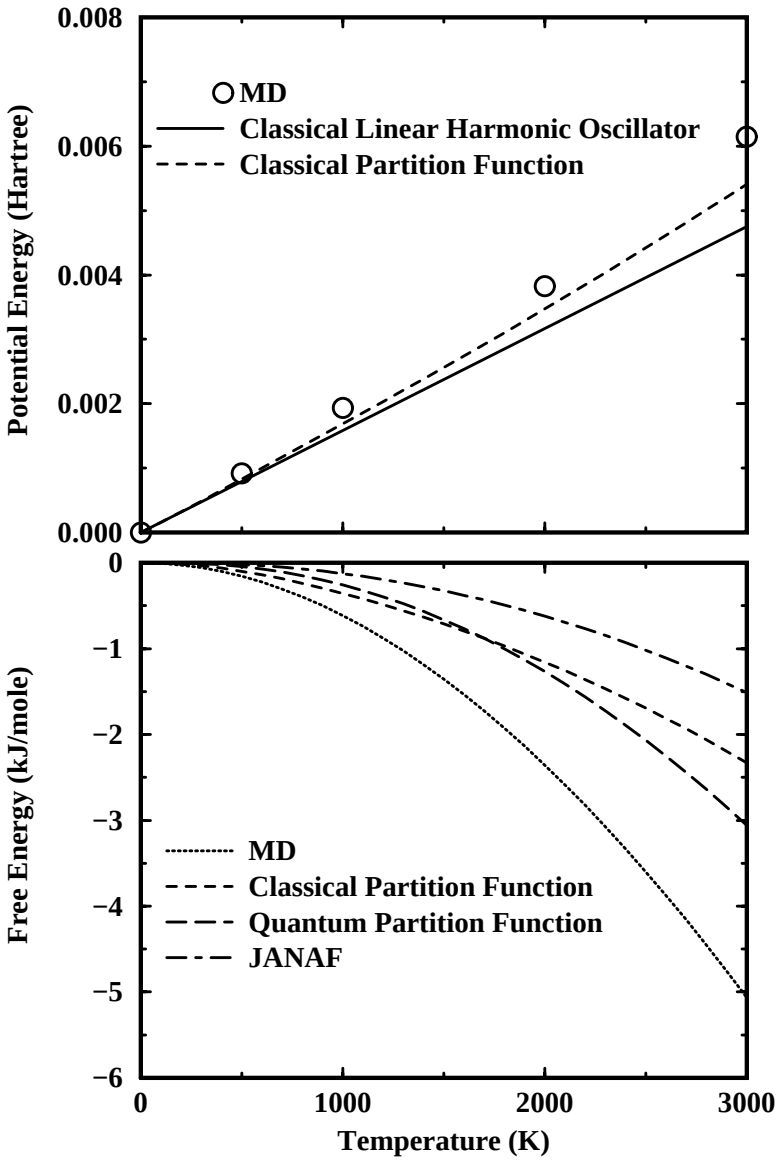

FIG. 6. Upper graph shows the average potential energies of Si_2 from molecular dynamics simulations and from the classical partition function. The solid line corresponds to a classical linear harmonic oscillator. The lower graph illustrates the anharmonic correction to the free energy of Si_2 from molecular dynamics simulations, the classical partition function, the quantum partition function, and JANAF [2].

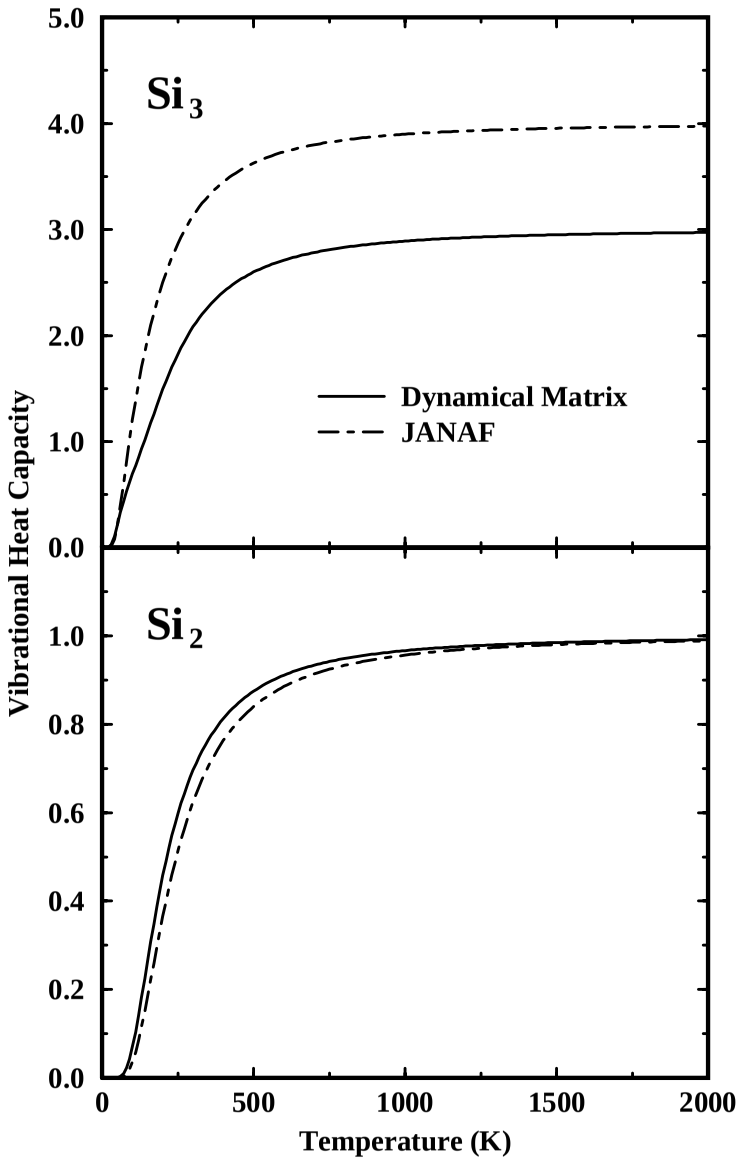

FIG. 7. Vibrational contributions to the dimensionless heat capacities of Si_2 and Si_3 from JANAF [2] and our work. These curves are based on Eq. (29) using the vibrational frequencies from the dynamical matrix and JANAF. The linear Si_3 cluster assumed in JANAF produces an additional vibrational mode as compared to the results for our non-linear structure.

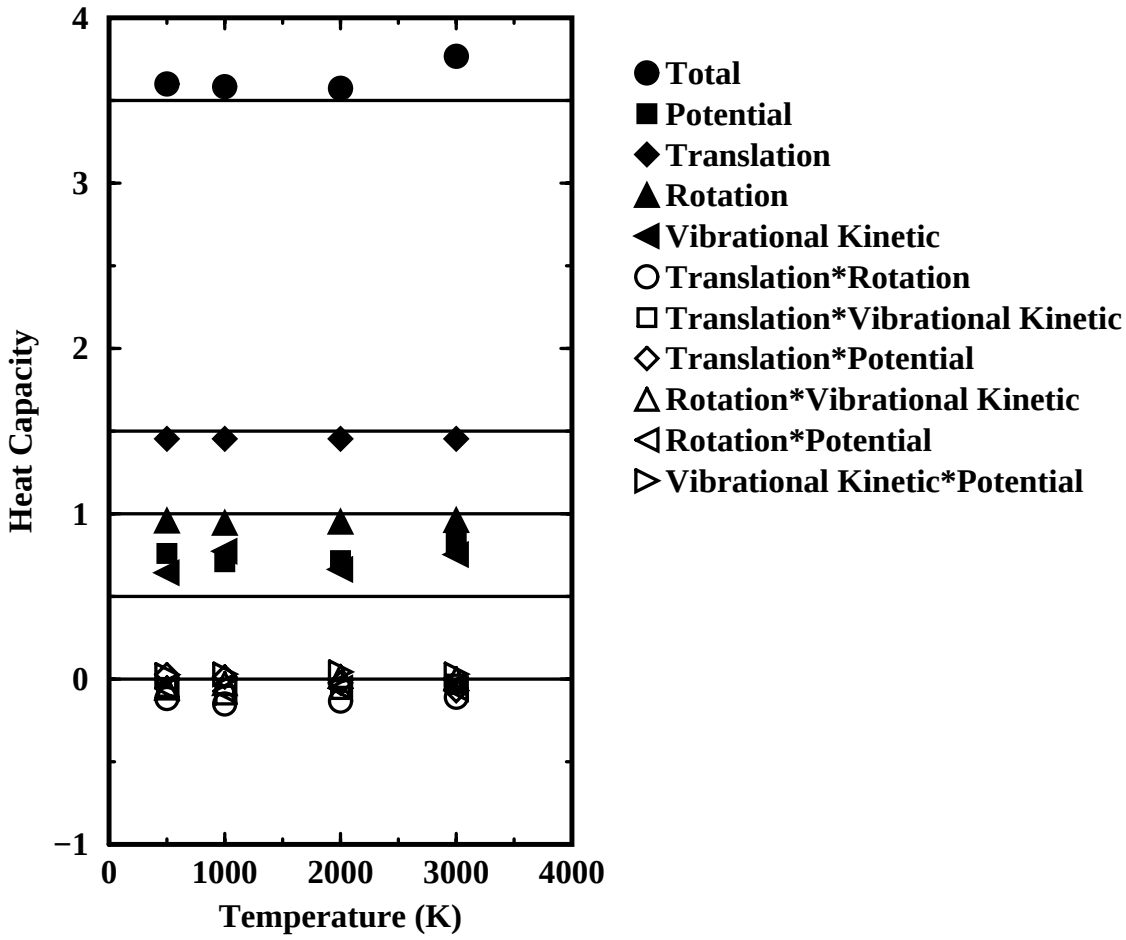

FIG. 8. Contributions to the dimensionless heat capacity of Si_2 from molecular dynamics simulations and Eq. (10). The filled and open symbols correspond to the variances and covariances, respectively, of each contribution to the energy. The straight lines correspond to an ideal classical gas of clusters that vibrate as linear harmonic oscillators and rotate as rigid rotators.

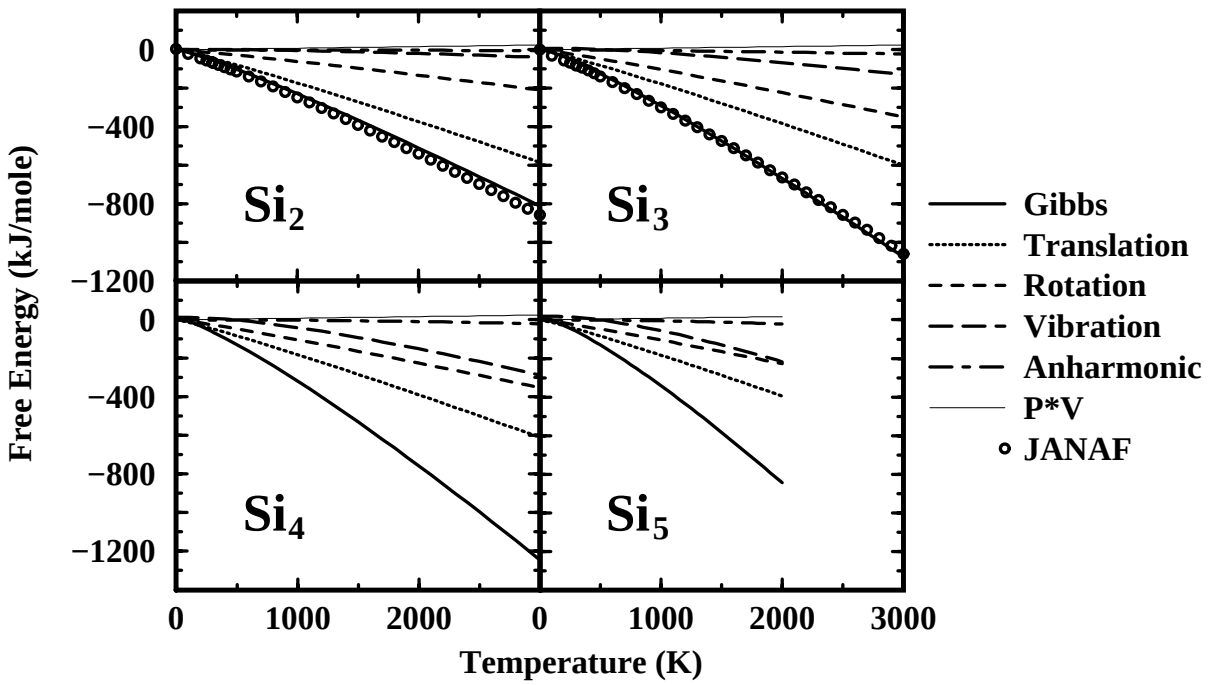

FIG. 9. Gibbs free energy and components (kcal/mole) for Si_2 through Si_5 at 1 bar from molecular dynamics simulations. The lines are based on the current work. The open circles are taken from the JANAF tables.